Letter

Concentric ring patterns beyond Turing instability

M. G. Clerc ⬡, S. Echeverria-Alar ⬡, L. A. Letelier ⬡, and C. Núñez-Barra ⬡

Departamento de Física and Millennium Institute for Research in Optics, Facultad de Ciencias Físicas y Matemáticas, Universidad de Chile, Casilla 487-3, Santiago, Chile

Various out-of-equilibrium physical systems exhibit concentric ring patterns. However, these patterns are expected to be unstable due to the interaction of spatial modes. Here, we show that concentric ring patterns are stable beyond Turing instability. Based on a prototype pattern forming model, we show that these solutions are stable and identify the main ingredients for their stability: curvature, characteristic wavelength, and bistability. We further characterize the propagation of stable concentric ring patterns. Experimentally, we observe stable concentric ring patterns in an illuminated dye-doped liquid crystal cell with sufficiently high intensity. The formation of the concentric rings is in agreement with our predicted theoretical findings.

Physical systems, in thermodynamic equilibrium, are characterized by presenting homogeneous equilibria that are invariant by spatial and temporal translation. Nonequilibrium processes often lead to the formation of dissipative structures in nature [1–4]. These processes are characterized by permanently injecting and dissipating energy, momenta, and particles. When the injection of energy is small compared to the dissipation, equilibria are usually characterized by being uniform and stationary, similar to those observed in thermodynamic equilibrium. From a dynamical system point of view, these equilibria correspond to attractors. Increasing the energy injection, the homogeneous states can become unstable and develop a pattern formation through a spatial symmetry-breaking instability [1–6]. The formation of patterns such as mountains, dunes, plants, clouds, snowflakes, stalactites, and skin of mammalians, insects, fish, and seashells has drawn attention since the beginning of time [3–7]. Also, spatiotemporal effects in patterns have motivated theoretical and experimental studies in nonequilibrium physics [8–11]. The wavelength of the pattern is usually determined by two mechanisms: (i) external, such as the geometric properties of the system under study (width, thickness, etc.) [2–6], or (ii) internal, such as different coupling properties (transport, diffusion, diffraction, etc.) [2–6,12]. This last mechanism, of an intrinsic length, was proposed by Turing [12], and it has been a relevant topic of study in the nonlinear optics community [6,13–17].

At the onset of spatial instability, a general strategy to describe the dynamics of the pattern is achieved through an amplitude equation approach [3,4,6,18], where the amplitudes account for the critical modes that become unstable.

As a result of the nonlinear terms, the linearly unstable critical modes become saturated. This balance can give rise to stripe, hexagon, square, superlattice, labyrinthine, or quasicrystal patterns near the instability [3–7,18–20]. The striped patterns are understood, in isotropic systems, as the stable equilibrium of a single mode [3–5,18]. The direction of this pattern depends on the initial condition. Likewise, the square, hexagonal, and superlattice patterns are understood as stable equilibria between two, three, and several resonant modes, respectively [3–5,18,21]. Labyrinthine patterns are understood as a stable equilibrium of many disordered phase critical modes with similar wave numbers and magnitude of the amplitude. The labyrinths are locally dominated by a single mode [19]. Quasicrystals result from higher codimensional instabilities that include modes of different wavelengths [3–6,22]. Patterns with many coherent phase modes with the same wavelength and amplitude can generate concentric ring patterns (see Fig. 1). Patterns with concentric rings are observed in vegetation [23], fluid convection [24], molecular assembling [25], suspended liquid crystal films [26], laser irradiation at the solid/liquid interface [27], gas-discharge systems [28], bacteria colony formation [29], optically pumped semiconductor amplifiers [30], electroexplosion in a needle iron metal plate [31], evaporation-assisted formation of surface patterns [32], evaporation of colloidal nanoparticles in a confined cell [33], the far field of a photorefractive oscillator [20], and the photoisomerization process in liquid crystals [34]. Although concentric ring patterns are observed in various physical systems, they are unstable from the point of view of amplitude equations [35,36]. Therefore, the mechanism of origin of these patterns and their properties is not established.

This Letter aims to show that concentric ring patterns are stable beyond Turing instability, in the sense that the phenomenon occurs after (or before) a Turing instability, but not at the onset. Based on a prototype mathematical model of pattern formation, we show that these solutions are stable and identify the necessary ingredients for their stability.
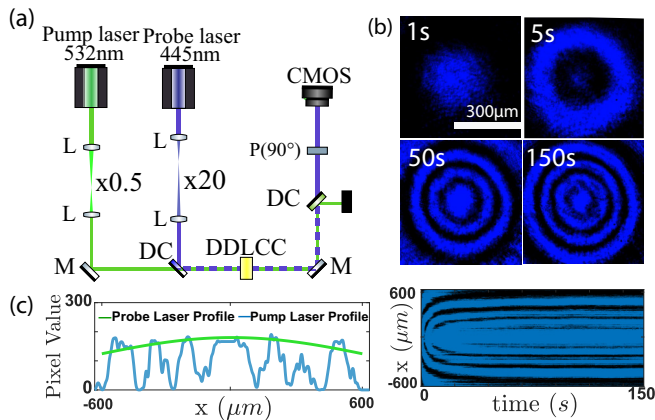
FIG. 1. Experimental observation of concentric ring patterns in a dye-doped liquid crystal sample under the effect of two parallel coherent beams. (a) Schematic representation of the experimental setup. A dye-doped liquid crystal cell (DDLCC) is irradiated by a 445-nm blue laser (BL, probing light beam) and illuminated by a 532-nm green laser (GL, excitation light beam). L, M, DC, and P account for lens, mirrors, dichroic crystals, and polarizer, respectively. DDLCC is monitored by a CMOS camera. (b) A horizontal cut of the spatiotemporal evolution (bottom panel) of an illuminated dye-doped liquid crystal cell. Panels show a temporal sequence of snapshots of the DDLCC cell. (c) Horizontal profile of the equilibrium concentric ring pattern.

Concentric ring patterns are observed in the region of bistability between uniform states and patterns. Close to Turing instability, when unstable concentric rings are forming, they are characterized by spreading so that the outer concentric rings aggregate. However, in the region where concentric ring patterns are stable, propagation is characterized by rings emerging from the center and pushing the ring structure. Hence, the propagation mechanisms of the modulated front are completely different. Notice that front propagation in both cases is controlled by curvature. Experimentally, we observe stable concentric ring patterns in an illuminated dye-doped liquid crystal cell with sufficiently high intensity. The formation and spread of the concentric rings are consistent with our theoretical findings.

Experimental setup and observations. Out-of-equilibrium liquid crystals exhibit complex spatial textures [37]. Traditional methods to keep liquid crystals out of equilibrium are the application of electric and magnetic fields, and thermal gradients. Likewise, they can be kept out of equilibrium with strong electromagnetic fields. In addition, a nonintense light beam can be used to drive liquid crystals out of equilibrium. To do this, liquid crystals can be doped with photosensitive molecules [38], which can change their molecular structure upon receiving a photon with a particular frequency (photoisomerization). In turn, the rotations of these light-sensitive molecules cause the oriented molecules of the liquid crystal to become disordered. Patterns induced by photoisomerization have been observed in a dye-doped nematic liquid crystal layer. This type of self-organization has been modeled by a reaction-diffusion system [34,39,40].

To study concentric ring patterns, we consider a dye-doped liquid crystal cell (DDLCC) under the effect of two parallel coherent beams at room temperature (18 °C). The sample is only photosensitive to one beam (excitation beam), and at the same time, the other is harmless (probing beam). Figure 1 illustrates the experimental setup diagram. The DDLCC undergoes a phototropic transition when it is irradiated by a light source in the absorption band of the guest dye [38]. We used a concentration of methyl red 0.5 wt % as the azo-dye guest doping a commercially available E7 nematic liquid crystal (host). The mixture was inserted into an antiparallel planar-aligned liquid crystal cell with a thickness of 25 μm (Instec). A 532-nm Verdi V-2 (Coherent) and 445-nm Cobolt 90 mW polarized laser were used as an exciting and probing irradiation light source to generate and observe a phototropic transition, respectively. Note that the green laser wavelength was close to the absorbance peak at 496 nm of the mixture, enabling us to trigger the isomerization and increase the amount of *cis* methyl red isomer. Two Kepler telescopes with a magnification of 0.5× and 20× were used to change the waist of the green and blue laser, respectively. A dichroic crystal (DC, high and low bandpass) is used to separate both beams and to monitor the DDLCC with a complementary metal-oxide-semiconductor (CMOS) camera. Before the CMOS camera, a polarizer was placed orthogonal to the polarization of the blue laser.

The camera displays a dark cell due to the polarizer when the DDLCC is illuminated with a blue probing light. When illuminating with the green laser with a power of the order of 300 mW (a waist of 0.56 mm), we initially observe a lightened circular area [see Fig. 1(b) at 1 s], which is later accompanied by a central circular dark spot that afterward becomes a dark propagating ring [see Fig. 1(b) at 5 s]. Then, a second spot appears in the center, which in turn becomes in another propagative ring. This process continues until four dark rings are established [see Fig. 1(b) at 150 s, and the video in the Supplemental Material [41]]. The lower panel of Fig. 1(b) summarizes the spatiotemporal evolution of the observed photoisomerization dynamics. Because the illuminated area is a Gaussian region, the ring patterns eventually stop, giving rise to a bull's-eye shape [cf. Fig. 1(b) at 150 s]. Figure 1(c) shows the horizontal profile of the equilibrium concentric ring pattern.

Theoretical descriptions. A prototype model of pattern formation is the Swift-Hohenberg equation [42], which is an isotropic, reflection symmetry, and real order parameter nonlinear equation deduced originally to describe the pattern formation on Rayleigh-Bénard convection [42]. This equation applies to a wide range of systems that undergo a spatial symmetry-breaking instability—often called Turing instability [2–4]—close to a second-order critical point marking the onset of a hysteresis loop, which corresponds to a Lifshitz point [4]. The Swift-Hohenberg equation reads

$$\partial_t u = \epsilon u - u^3 - \nu \nabla^2 u - \nabla^4 u, \qquad (1)$$

where $u = u(x, y, t)$ is a real scalar field, x and y are spatial coordinates, and t is time. Depending on the context in which this equation has been derived, the physical meaning of the scalar field $u = u(x, y, t)$ could be the electric field, deviation of molecular orientations, phytomass density, or chemical concentration, among others. The control or bifurcation parameter ϵ measures the input field amplitude, the

aridity parameter, or the chemical concentration. The parameter ν stands for the diffusion coefficient ($\nu < 0$); when this parameter is positive ($\nu > 0$), it induces an antidiffusion process, which is characterized by the emergence of patterns with a characteristic wavelength.

For sufficiently negative ϵ, the only stable state of this model Eq. (1) is the zero solution $u = 0$. When ϵ is increased or exceeds the critical value $\epsilon_{c1} = -\nu^2/4$, it exhibits a supercritical spatial instability (Turing instability) [3,4], which gives rise to stable stripe patterns with a $\sqrt{\nu/2}$ wave number. The zero unstable state presents a secondary instability for $\epsilon = 0$, giving rise to two new homogeneous uniform states $\pm\sqrt{\epsilon}$, which stabilize for $\epsilon = \epsilon_{c2} \equiv \nu^2/8$. Then, for $\epsilon > \epsilon_{c2}$, the system presents bistability between the uniform solutions $\pm\sqrt{\epsilon}$ and the pattern states. Figure 2(e) depicts the bifurcation diagram of the Swift-Hohenberg equation (1). Numerically, we have considered the uniform state $-\sqrt{\epsilon}$, and we have perturbed it locally with a Gaussian [with a width of the pattern wavelength—see Fig. 2(d)]. Depending on ϵ, we observe different behaviors. In the region where uniform states are unstable ($\epsilon_{c1} \leqslant \epsilon \leqslant 0$), we observe the propagation of unstable concentric rings [cf. Fig. 2(a)] [24]. This propagation is characterized by the appearance of outer rings that are attached. When ϵ is increased, the previous scenario changes. We observe similar propagation, but of stable concentric ring patterns. In Fig. 2(e), we have characterized the parameter space where this behavior is observed and called it *outside ringing*. Further increasing ϵ, and the system being in the bistability region, propagation is characterized by rings emerging from the center and pushing the concentric ring structure [see Fig. 2(b)]. We have termed this region *inside ringing*. When ϵ is increased even more, the system does not exhibit the formation of a concentric ring pattern, but rather the propagation of one homogeneous state over the other. We have named this region *inflation* [cf. Fig. 2(c)]. Further increasing ϵ, the initial perturbation stabilizes in a localized structure [see Fig. 2(d)]. In addition, we have considered numerical simulations in a circular geometry to avoid edge effects, and study the stability of concentric ring patterns. The lower panels (I) and (II) of Fig. 2(e) show stable concentric ring patterns. Note that stable concentric ring patterns are observed beyond Turing instability ($\epsilon > \epsilon_{c1}$, $\epsilon < \epsilon_{c2}$, and $\epsilon > \epsilon_{c2}$). This could be related to a shift of the Turing boundary due to the axisymmetric (radial) restriction on the initial condition. Numerical simulations were conducted with the Runge-Kutta fourth-order algorithm for time integration and a finite-difference scheme for spatial discretization.

To shed light on concentric ring patterns, we consider a one-dimensional model that contains the necessary ingredients (curvature, bistability, and a characteristic wavelength) to observe these patterns and their dynamics. Considering that patterns are rotation invariant, we can propose the following ansatz $u(x, y, t) = u(r, t)$, where r is the radial coordinate. Thus, Eq. (1) reads

$$\partial_t u = \epsilon u - u^3 - \nu\left(\partial_{rr} + \frac{\partial_r}{r}\right)u$$
$$- \left(\partial_{rrrr} + 2\frac{\partial_{rrr}}{r} - 2\frac{\partial_{rr}}{r^2} + \frac{\partial_r}{r^3}\right)u, \qquad (2)$$
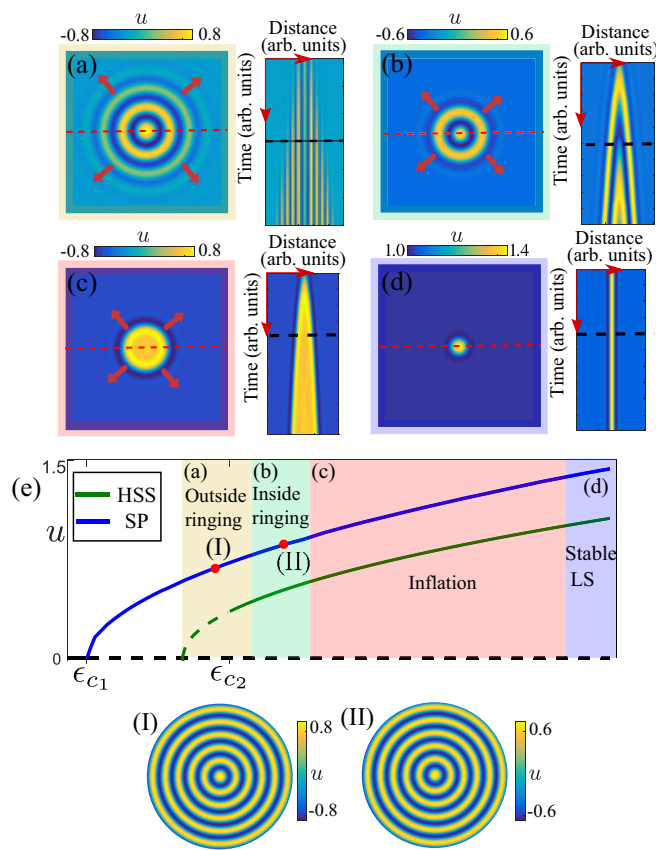

FIG. 2. Numerical observations of concentric ring patterns in the Swift-Hohenberg Eq. (1) for $\nu = 1$. Different concentric ring patterns are observed considering the homogeneous state $-\sqrt{\epsilon}$ and perturbing it with a small Gaussian. (a) Outside ringing: The pattern propagation is characterized by the appearance of attached outer rings. (b) Inside ringing: The pattern propagation is characterized by rings emerging from the center and pushing the concentric ring structure. (c) Inflation: Front propagation of one homogeneous state over the other. (d) Stable localized structures. The right panels illustrate the spatiotemporal evolution of the middle line in the two-dimensional simulations (segmented red line). The left panels depict the surface plots obtained at the instant represented by the black dashed line on the spatiotemporal diagram. (e) Bifurcation diagram of the Swift-Hohenberg Eq. (1): Maximum value of u vs ϵ. The green line corresponds to the uniform state $\sqrt{\epsilon}$ (HSS, homogeneous steady state), the blue curve stands for stripe patterns (SP), and the black line represents the zero solution. Segmented and solid lines indicate that the corresponding state is unstable and stable, respectively. The lower panels (I) and (II), which correspond to the red solid circles, show stable concentric ring patterns.

which is a one-dimensional Swift-Hohenberg model with curvature corrections inherent to two dimensions. The curvature effects are controlled by the terms proportional to the inverse of a power of r in Eq. (2). This model has uniform solutions $\mu = \{0, \pm\sqrt{\epsilon}\}$ and one-dimensional patterns. Note that these patterns correspond to concentric ring states. $\epsilon = \epsilon_{c1} = -\nu^2/4$ accounts for the Turing instability (supercritical spatial instability) for Eq. (2) [3,4]. In the case when one ignores the curvature effects (standard one-dimensional Swift-Hohenberg model), patterns propagate through the emergence of spatial
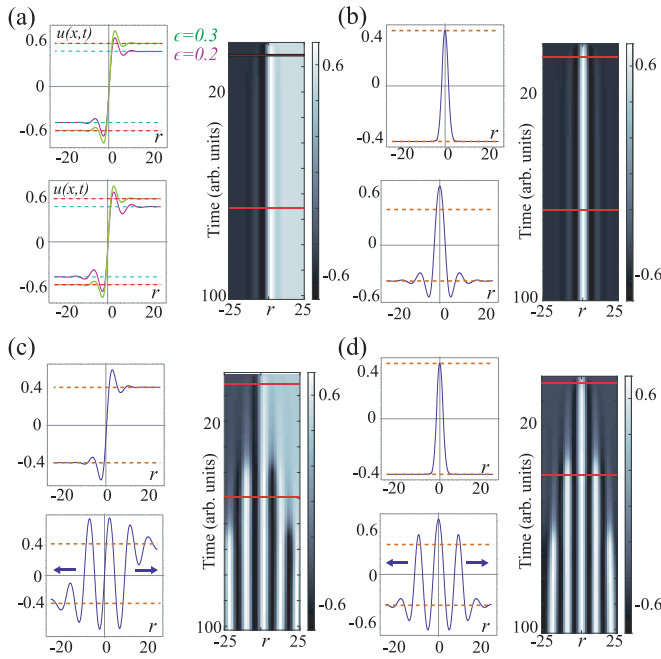
FIG. 3. Domain walls and localized structures of the one-dimensional Swift-Hohenberg Eq. (2) for $\nu = 1$, and without curvature corrections. (a) Domain wall profile and spatiotemporal evolution between symmetrical uniform states $u = \pm\sqrt{\epsilon}$ for $\epsilon = \{0.2, 0.3\}$. (b) Profiles of localized structures and spatiotemporal evolution ($\epsilon = 0.2$). (c) Pattern propagation from a domain wall solution ($\epsilon = 0.15$) or a (d) localized structure ($\epsilon = 0.15$). The red lines on the spatiotemporal diagram show the instant where the profiles are obtained. The dashed horizontal lines account for the homogeneous equilibria. The domain of integration is from $r = -25$ to $r = 25$.

oscillations at the end of the pattern. Figure 3 illustrates pattern propagation in the absence of curvature, by integrating Eq. (2) in the whole spatial range (negative and positive values of r). This behavior is similar to that observed in concentric ring patterns in two dimensions in the outside ringing region; see Fig. 2(e). We consider ϵ in the region of bistability between uniform and pattern states. In this parameter region, the system has a domain wall solution that connects two symmetric states [see Fig. 3(a)]. The damped spatial oscillation amplitudes increase with ϵ. Likewise, the model Eq. (2), without curvature effects, has localized structures, for higher values of ϵ, supported by homogeneous states [see Fig. 3(b)]. For lower values of ϵ, the pattern state becomes more stable than the homogeneous one. Then, the pattern begins to propagate from the domain wall center or from the localized structure [see the bottom panels of Figs. 3(c) and 3(d), respectively].

The above scenario changes radically when one considers the curvature effects. Starting from a localized structure in the center of the numerical integration domain, for ϵ in the outside ringing region, we observe pattern propagation through the emergence of spatial oscillations outside the pattern [see Fig. 4(a)], as in the case without curvature effects. However, by increasing ϵ (inside ringing region), the propagation changes drastically. Now, spatial oscillations created in the center of the integration domain drive the propagation, which propagates outward, and subsequently gives rise to new
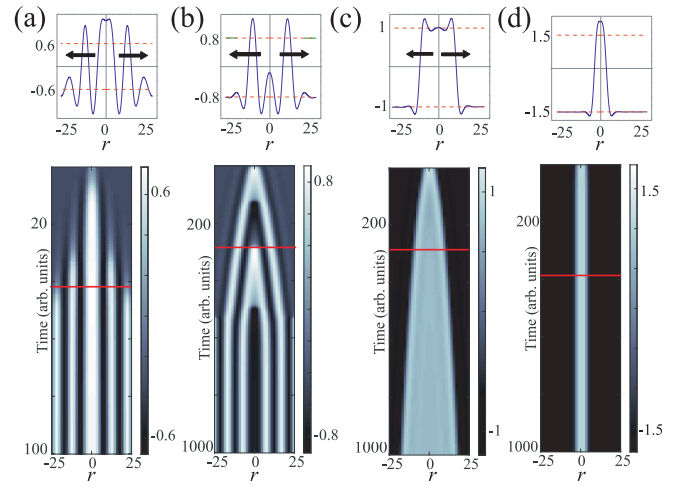

FIG. 4. Pattern propagation and profiles from a localized structure of the one-dimensional Swift-Hohenberg model Eq. (2) for $\nu = 1$. (a) Pattern propagation for $\epsilon = 0.1$ by including spatial oscillations in the outer part of the pattern. (b) Pattern propagation for $\epsilon = 0.2$ characterized by spatial oscillations that emerge from the center and push the pattern structure outward. (c) Front propagation of one homogeneous state over the other, for $\epsilon = 0.5$. (d) Stable localized structures for $\epsilon = 0.9$. The red lines on the spatiotemporal diagrams show the instant where the profiles are obtained. The dashed horizontal lines account for the homogeneous equilibria. The domain of integration is from $r = 0$ to $r = 25$, and then reflected at $r = 0$.

oscillations in the center [cf. Fig. 4(b)]. This type of propagation is similar to the one observed experimentally [see Fig. 1(b)]. When ϵ is increased even more, we observe, as a consequence of the curvature, that one homogeneous state invades the other as illustrated in Fig. 4(c). Notice that the speed of the fronts is constantly decelerating. This observed dynamical behavior is consistent with what we have called the inflation region in Fig. 2(e). By further increasing ϵ, the localized structure is stable, and propagation of patterns or homogenous states is not observed [see Fig. 4(d)]. The solutions of Eq. (2) shown in Fig. 4 were numerically integrated for $r > 0$, and then reflected at $r = 0$. In brief, the effects of curvature and bistability (uniform and pattern state) control and stabilize the propagation mechanisms of concentric ring patterns. The transition between the *inflation* mode and a stationary localized structure has been reported in a previous work [43]. There, a Swift-Hohenberg model was used to explore the phase domain dynamics. By a minimization principle, a local velocity-curvature relationship was proposed. Note that in the cases of *inside* and *outside* ringing [cf. Fig. 2(e)], the local approximation is invalid, and the ring dynamics is governed by nonlocal interactions.

In conclusion, we have shown that concentric ring patterns are stable beyond Turing instability. To observe these concentric ring patterns, the bistability of patterns and homogeneous states in an isotropic medium is required. Based on a prototype model, the Swift-Hohenberg equation, we show that these solutions are stable and identify the ingredients for their stability. Close to the Turing instability, the concentric rings are unstable due to the interaction of spatial modes. Then, beyond the Turing instability, the concentric ring

patterns can be stabilized. We propose a mechanism of pattern formation, inside ringing, which is triggered by curvature. Experimentally, we observed stable concentric ring patterns in an illuminated dye-doped liquid crystal cell with sufficiently high intensity. The formation of the concentric ring patterns is in agreement with our theoretical findings in the inside ringing region.

[1] P. Glansdorff and I. Prigogine, *Thermodynamic Theory of Structures. Stability and Fluctuations* (Wiley, New York, 1971).

[2] G. Nicolis and I. Prigogine, *Self-Organization in Nonequilibrium Systems* (Wiley, New York, 1977).

[3] L. M. Pismen, *Patterns and Interfaces in Dissipative Dynamics* (Springer, Berlin, 2006).

[4] M. Cross and H. Greenside, *Pattern Formation and Dynamics in Non-Equilibrium Systems* (Cambridge University Press, New York, 2009).

[5] R. B. Hoyle, *Pattern Formation: An Introduction to Methods* (Cambridge University Press, Cambridge, U.K., 2006).

[6] F. T. Arecchi, S. Boccaletti, and P. Ramazza, Pattern formation and competition in nonlinear optics, Phys. Rep. **318**, 1 (1999).

[7] J. D. Murray, *Mathematical Biology* (Springer, New York, 1990).

[8] P. Coullet, T. Frisch, and F. Plaza, Sources and sinks of wave patterns, Physica D **62**, 75 (1993).

[9] P. Coullet, D. Daboussy, and J. R. Tredicce, Optical excitable waves, Phys. Rev. E **58**, 5347 (1998).

[10] T. Frisch, S. Rica, P. Coullet, and J. M. Gilli, Spiral Waves in Liquid Crystal, Phys. Rev. Lett. **72**, 1471 (1994).

[11] P. Coullet, S. Fauve, and E. Tirapegui, Large scale instability of nonlinear standing waves, J. Phys. Lett. **46**, 787 (1985).

[12] A. Turing, The chemical basis of morphogenesis, Philos. Trans. R. Soc. B **237**, 37 (1952).

[13] S. A. Akhmanov, M. A. Vorontsov, and V. Yu. Ivanov, Large-scale transverse nonlinear interactions in laser beams - New types of nonlinear waves, generation of "optical turbulence", Pis'ma Zh. Eksp. Teor. Fiz. **47**, 611 (1988).

[14] S. A. Akhmanov, M. A. Vorontsov, V. Yu. Ivanov, A. V. Larichev, and N. I. Zheleznykh, Controlling transverse-wave interactions in nonlinear optics: generation and interaction of spatiotemporal structures, J. Opt. Soc. Am. B **9**, 78 (1992).

[15] N. N. Rosanov, *Spatial Hysteresis and Optical Patterns* (Springer, Berlin, 2002).

[16] K. Staliunas and V. J. Sanchez-Morcillo, *Transverse Patterns in Nonlinear Optical Resonators* (Springer, Berlin, 2003).

[17] M. Tlidi, K. Staliunas, K. Panajotov, A. G. Vladimirov, and M. G. Clerc, Localized structures in dissipative media: from optics to plant ecology, Philos. Trans. R. Soc. A **372**, 20140101.

[18] A. C. Newell, T. Passot, and J. Lega, Order parameter equations for patterns, Annu. Rev. Fluid Mech. **25**, 399 (1993).

[19] S. Echeverría-Alar and M. G. Clerc, Labyrinthine patterns transitions, Phys. Rev. Res. **2**, 042036(R) (2020).

[20] K. Staliūnas, G. Šlekys, and C. O. Weiss, Nonlinear Pattern Formation in Active Optical Systems: Shocks, Domains of Tilted Waves, and Cross-Roll Patterns, Phys. Rev. Lett. **79**, 2658 (1997).

[21] A. O. Leon, M. G. Clerc, and S. Coulibaly, Dissipative structures induced by spin-transfer torques in nanopillars, Phys. Rev. E **89**, 022908 (2014).

[22] M. C. Walters, P. Subramanian, A. J. Archer, and R. Evans, Structural crossover in a model fluid exhibiting two length scales: Repercussions for quasicrystal formation, Phys. Rev. E **98**, 012606 (2018).

[23] R. Berg, Age determination of eels, *Anguilla anguilla* (L): comparison of field data with otolith ring patterns, J. Fish Biol. **26**, 537 (1985).

[24] Y. Hu, R. E. Ecke, and G. Ahlers, Behavior of Focus Patterns in Low Prandtl Number Convection, Phys. Rev. Lett. **72**, 2191 (1994).

[25] H. Maeda, An Atomic Force Microscopy Study of Ordered Molecular Assemblies and Concentric Ring Patterns from Evaporating Droplets of Collagen Solutions, Langmuir **15**, 8505 (1999).

[26] D. R. Link, L. Radzihovsky, G. Natale, J. E. Maclennan, N. A. Clark, M. Walsh, S. S. Keast, and M. E. Neubert, Ring-Pattern Dynamics in Smectic-C^* and Smectic-C_A^* Freely Suspended Liquid Crystal Films, Phys. Rev. Lett. **84**, 5772 (2000).

[27] K. Katayama, H. Yonekubo, and T. Sawada, Formation of ring patterns surrounded by ripples by single-shot laser irradiation with ultrashort pulse width at the solid/liquid interface, Appl. Phys. Lett. **82**, 4244 (2003).

[28] E. L. Gurevich, A. L. Zanin, A. S. Moskalenko, and H.-G. Purwins, Concentric-Ring Patterns in a Dielectric Barrier Discharge System, Phys. Rev. Lett. **91**, 154501 (2003).

[29] H. Shimada, T. Ikeda, J. Wakita, H. Itoh, S. Kurosu, F. Hiramatsu, M. Nakatsuchi, Y. Yamazaki, T. Matsuyama, and M. Matsushita, Dependence of local cell density on concentric ring colony formation by bacterial species Bacillus subtilis, J. Phys. Soc. Jpn. **73**, 1082 (2004).

[30] S. Barbay, Y. Ménesguen, X. Hachair, L. Leroy, I. Sagnes, and R. Kuszelewicz, Incoherent and coherent writing and erasure of cavity solitons in an optically pumped semiconductor amplifier, Opt. Lett. **31**, 1504 (2006).

[31] Vandana and P. Sen, Concentric ring patterns in needle-plate exploding systems, J. Phys.: Condens. Matter **19**, 016009 (2007).

[32] W. Sun and F. Q. Yang, Evaporation-assisted formation of surface patterns from polymer solutions via copper tubes, Express Polym. Lett. **12**, 699 (2018).

[33] V. K. Vlasko-Vlasov, M. Sulwer, E. V. Shevchenko, J. Parker, and W. K. Kwok, Ring patterns generated by an expanding colloidal meniscus, Phys. Rev. E **102**, 052608 (2020).

[34] M. G. Clerc, G. Gonzalez-Cortes, P. I. Hidalgo, L. A. Letelier, M. J. Morel, and J. Vergara, Light-induced ring pattern in a dye-doped nematic liquid crystal, Appl. Sci. **11**, 5285 (2021).

[35] D. Lloyd and B. Sandstede, Localized radial solutions of the Swift-Hohenberg equation, Nonlinearity **22**, 485 (2009).

[36] C. Castillo-Pinto, M. G. Clerc, and G. González-Cortés, Extended stable equilibrium invaded by an unstable state, Sci. Rep. **9**, 15096 (2019).

[37] I. Dierking, *Textures of Liquid Crystals* (Wiley-VCH, Weinheim, 2003).

[38] I. C. Khoo, *Liquid Crystals* (Wiley, Hoboken, NJ, 2007).

[39] I. Andrade-Silva, U. Bortolozzo, M. G. Clerc, G. Gonzalez-Cortes, S. Residori, and M. Wilson, Spontaneous light-induced Turing patterns in a dye-doped twisted nematic layer, Sci. Rep. **8**, 12867 (2018).

[40] I. Andrade-Silva, U. Bortolozzo, C. Castillo-Pinto, M. G. Clerc, G. Gonzalez-Cortes, S. Residori, and M. Wilson, Dissipative structures induced by photoisomerization in a dye-doped nematic liquid crystal layer, Philos. Trans. R. Soc. A **376**, 20170382 (2018).

[41] See Supplemental Material at http://link.aps.org/supplemental/10.1103/PhysRevResearch.5.L012007 for a video showing the emergence and pattern of concentric rings observed in a dye-doped liquid crystal cell illuminated with two parallel light beams.

[42] J. Swift and P. C. Hohenberg, Hydrodynamic fluctuations at the convective instability, Phys. Rev. A **15**, 319 (1977).

[43] K. Staliunas and V. J. Sanchez-Morcillo, Dynamics of phase domains in the Swift-Hohenberg equation, Phys. Lett. A **241**, 28 (1998).